Probing Electron-Induced Bond Cleavage at the Single-Molecule Level Using DNA Origami Templates

Adrian Keller,[†,‡,△,*] Ilko Bald,[†,△,▽,*] Alexandru Rotaru,[†,§] Emilie Cauët,[⊥] Kurt V. Gothelf,[†,∥] and Flemming Besenbacher[†,#]

[†]Interdisciplinary Nanoscience Center (iNANO) and Danish National Research Foundation: Centre for DNA Nanotechnology (CDNA), Aarhus University, 8000 Aarhus C, Denmark, [‡]Institute of Ion Beam Physics and Materials Research, Helmholtz-Zentrum Dresden-Rossendorf, 01328 Dresden, Germany, [§]Center of Advanced Research in Bionanoconjugates and Biopolymers, "Petru Poni" Institute of Macromolecular Chemistry, 700487 Iasi, Romania, [⊥]Service de Chimie Quantique et Photophysique, Université Libre de Bruxelles, 1050 Brussels, Belgium, [∥]Department of Chemistry, Aarhus University, 8000 Aarhus C, Denmark, and [#]Department of Physics and Astronomy, Aarhus University, 8000 Aarhus C, Denmark. [△]These authors contributed equally to this work. [▽]Present address: Department of Chemistry—Physical Chemistry, University of Potsdam, 14476 Potsdam, Germany.

ABSTRACT

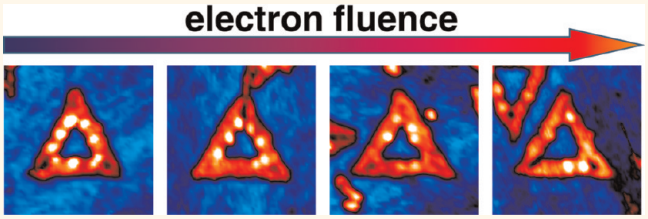

Low-energy electrons (LEEs) play an important role in nanolithography, atmospheric chemistry, and DNA radiation damage. Previously, the cleavage of specific chemical bonds triggered by LEEs has been demonstrated in a variety of small organic molecules such as halogenated benzenes and DNA nucleobases. Here we present a strategy that allows for the first time to visualize the electron-induced dissociation of single chemical bonds within complex, but well-defined self-assembled DNA nanostructures. We employ atomic force microscopy to image and quantify LEE-induced bond dissociations within specifically designed oligonucleotide targets that are attached to DNA origami templates. In this way, we use a highly selective approach to compare the efficiency of the electron-induced dissociation of a single disulfide bond with the more complex cleavage of the DNA backbone within a TT dinucleotide sequence. This novel technique enables the fast and parallel determination of DNA strand break yields with unprecedented control over the DNA's primary and secondary structure. Thus the detailed investigation of DNA radiation damage in its most natural environment, *e.g.*, DNA nucleosomes constituting the chromatin, now becomes feasible.

KEYWORDS: DNA origami · low-energy electrons · atomic force microscopy · DNA radiation damage · *ab initio* calculations

The potential of low-energy electrons (LEEs) to induce chemical reactions is well known[1] and plays a key role in many natural and technological processes ranging from stratospheric ozone depletion[2] to DNA radiation damage[3] to nanofabrication.[4] LEEs can be used to break and re-form specific chemical bonds in molecules, which is employed for instance in chemical lithography,[5,6] for modification and functionalization of surfaces,[7] and for the fabrication of novel materials such as nanomembranes[8] and nanocrystalline graphene sheets.[9] At low energies (<12 eV) selected chemical bonds can be broken by simply tuning the electron energy due to the resonant character of the dissociative electron attachment (DEA) process.[10,11] At the single-molecule level LEE-induced reactions can be triggered and observed by scanning tunneling microscopy.[12−16] However, these studies are usually restricted to small, simple molecules and often require cryogenic temperatures.

On the other hand, LEEs are also produced in abundance along the track of high-energy radiation such as X-rays and γ-rays through biological tissue.[17] These secondary electrons are held responsible for a large fraction of the resulting damage to the DNA in the cell nucleus.[18] Even LEEs with kinetic energies well below the ionization limit of most organic molecules (*i.e.*, $E \leq 10$ eV) can induce single (SSBs) and double strand breaks (DSBs) in plasmid DNA through the DEA mechanism.[3,19] The quantification of LEE-induced strand breaks in dependence of the DNA sequence and topology, however, still represents an experimental challenge.[20,21]

Here we present a novel and versatile method that allows for the quantitative assessment of LEE-induced bond dissociation at the single-molecule level. This approach is based on detailed atomic force microscopy (AFM) analysis of well-defined DNA targets attached to DNA origami templates and can be used to study both the

* Address correspondence to a.keller@hzdr.de; bald@uni-potsdam.de.

Received for review March 12, 2012 and accepted April 17, 2012.

Published online April 17, 2012
10.1021/nn3010747

dissociation of selected chemical bonds and the strand cleavage in complex DNA structures of predefined sequence and topology.

In the DNA origami technique a long, single-stranded DNA (ssDNA) scaffold is folded into any desired shape by a set of designed short synthetic oligonucleotides, called staple strands.[22] Each staple strand can be extended to protrude from the DNA origami surface and can be individually functionalized, resulting in a well-defined DNA template with more than 200 individually addressable sites located 6 nm apart from each other.[22,23] The protruding strands can be systematically modified by introduction of functional linkers into the DNA's backbone[24,25] and by variation of the nucleobase sequence and topology. By using AFM to visualize the individual protruding strands, bond dissociation can thus be evaluated quantitatively on a single-molecule level as a function of the irradiation parameters (electron fluence, electron energy) and the target structure (linker type, DNA nucleobase sequence, DNA hybridization state). Furthermore, several differently modified DNA strands can be attached to the same DNA origami template, which allows us to quantify the dissociation yields of multiple target species in a single irradiation experiment.

In order to demonstrate the power of this new approach, we study the LEE-induced dissociation of a specific disulfide bond at the single-molecule level and compare it quantitatively to the more complex cleavage of the DNA's 2′-deoxyribose phosphate backbone in a thymine (T) dimer. Disulfide bridges are formed between two cysteine amino acids and have been suggested to be the most sensitive target for LEE attack on proteins.[26] The LEE-induced cleavage of the S−S bond thus plays an important role in protein sequencing by mass spectrometry[27] and radiation-induced structural alterations during protein crystallography[28] and can be further exploited in chemical lithography.[13] In addition, LEE-induced fragmentation of proteins in the cell nucleus (*e.g.*, in the histones) is considered a secondary source of DNA radiation damage due to the formation of reactive radicals in the close vicinity of the DNA.[29]

RESULTS AND DISCUSSION

Strategy for the Quantification of LEE-Induced Bond Cleavage. The detailed strategy pursued to study LEE-induced bond breaking on DNA origami structures is outlined in Figure 1. We have used the triangular origami design by Rothemund,[22] which was decorated with protruding DNA strands (see Supporting Information for details). The protruding strands are functionalized with biotin (Bt), which has a high binding affinity to the protein streptavidin (SAv), which appears as a bright protrusion in AFM images. The observation of

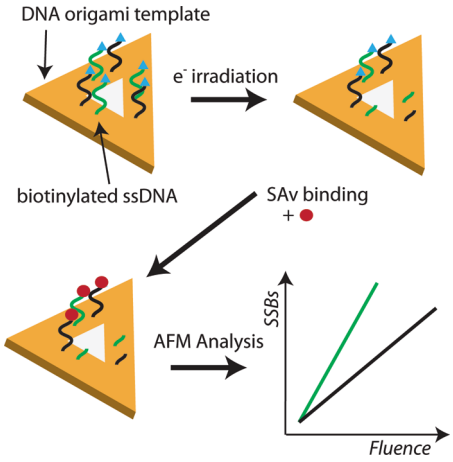

Figure 1. Scheme of the experimental sequence used to quantify electron-induced bond dissociation. Triangular DNA origami structures featuring six protruding strands with two different target structures (indicated in green and black) are irradiated with low-energy electrons.

such a bright protrusion at one of the predefined positions of the protruding DNA strands strongly indicates the presence of an intact strand.[24,25] For the detection of LEE-induced strand cleavage the following sequence of experiments is carried out: (i) Adsorption of DNA origami structures with biotinylated protruding strands without SAv markers onto SiO_2/Si surfaces; (ii) irradiation of the DNA origami sample in ultrahigh vacuum (UHV) with LEEs of defined energy and fluence; (iii) addition of SAv to visualize the intact protruding strands; (iv) AFM imaging of an irradiated and a nonirradiated control sample followed by statistical analysis based on the number of specifically bound SAv markers per DNA origami; (v) determination of the number of strand breaks as a function of target structure and electron fluence Φ, which is the number of electrons N per unit surface area A, $\Phi = N/A$.

LEE-Induced Dissociation of a Single Disulfide Bond. Figure 2a shows an AFM image of nonirradiated triangular DNA origami templates with nine protruding DNA single strands (design D1) after SAv binding. The protruding strands have the sequence 3′-SS-TT-Bt-5′ with SS being a disulfide linker ($(CH_2)_6SS(CH_2)_6$) introduced into the backbone of the DNA. In the following, S−S bond cleavage induced by 18 eV electrons is studied.

The AFM images in Figure 2b−d show that LEE irradiation at different fluences of 18 eV electrons leads to a continuous decrease of the number of specifically bound SAv molecules on the DNA origami template, indicating the cleavage of the protruding strands. The number of SSBs (in %) is plotted as a function of electron fluence in Figure 2e. The fraction of cleaved strands increases linearly with fluence until a saturation is observed at a fluence $\Phi \approx 4 \times 10^{12}$ cm^{-2}. Such saturation is generally observed in the LEE irradiation of DNA solids[3,30] and can be attributed to a slow charge

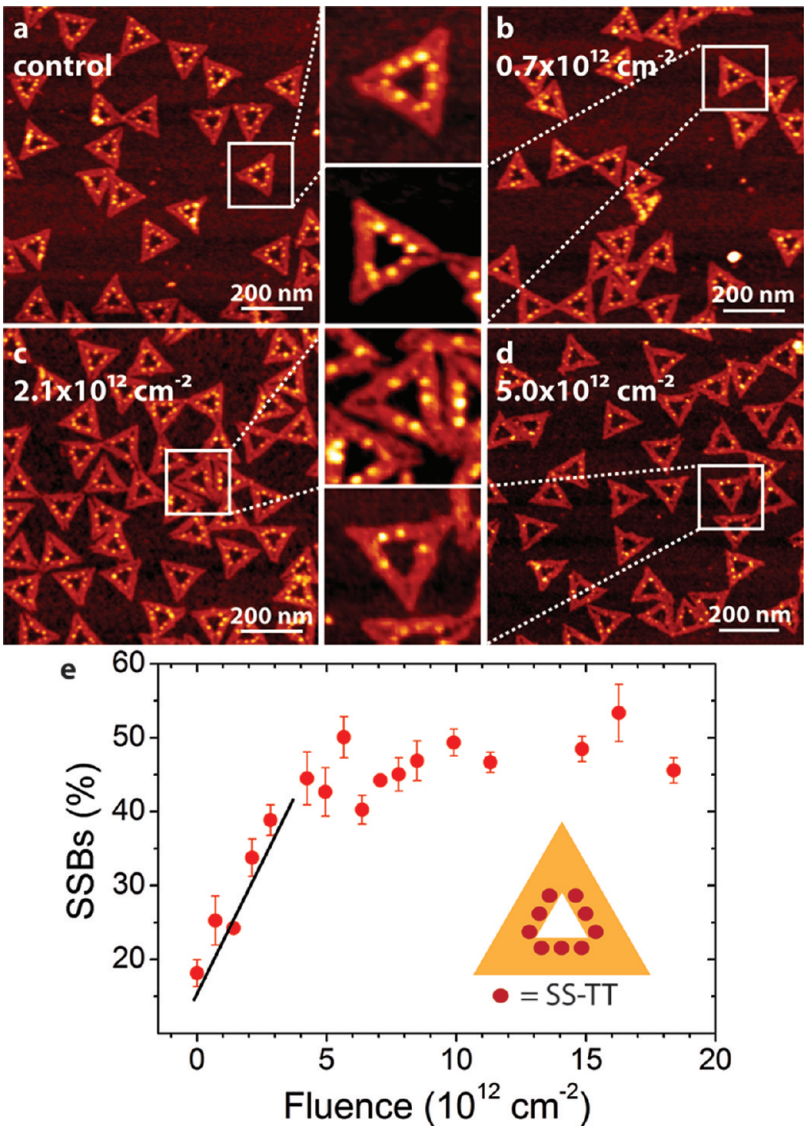

Figure 2. Irradiation of DNA origami templates with nine disulfide-containing strands. (a) AFM image of a nonirradiated control sample. The protruding strands have the sequence SS-TT. The templates are adsorbed on silicon and were exposed to SAv. A SAv binding efficiency of 80−90% was determined. (b−d) Samples irradiated with different fluences of 18 eV electrons. The number of specifically bound SAv decreases with electron fluence, indicating LEE-induced strand breaks. (e) Number of SSBs (in %) *vs* electron fluence for design D1 (shown in the inset).

accumulation in the DNA origami structures or the SiO_2 surface upon irradiation, which finally leads to a repulsion of the incident electrons. On the other hand, LEEs can induce chemical modifications in the DNA molecules such as interstrand cross-links that may prevent the subsequent detection of the strand breakage. The probability of one electron inducing a strand break is given by the slope of the linear response in the low-fluence regime and can be expressed as the dissociation yield (DY), *i.e.*, the number of detected strand breaks per incident electron and DNA origami. The fit to the linear response regime (black line in Figure 2e) reveals a DY of 1.0×10^{-3}.

Figure 3a shows the histogram of the number of observed intact protruding strands per DNA origami for a nonirradiated control sample. The histogram follows a single Gaussian distribution that is centered at 7.6 intact protruding strands. This value thus corresponds to a finite binding efficiency of SAv to Bt of about 84%. After irradiation with a fluence $\Phi = 1.6 \times 10^{13}$ cm^{-2} (Figure 3b), *i.e.*, within the saturation regime, the histogram shifts to a lower value of 4.2 due to LEE-induced strand cleavage. Interestingly, the width of the distribution does not change significantly during irradiation (2.8 *vs* 3.0), indicating that it is solely governed by the SAv−Bt binding.

In the above experiments, the DNA origami templates can adsorb in two geometries, *i.e.*, with the protruding strands facing toward the solution (face up) or toward the surface (face down). In the latter case, the protruding strands will be buried between the DNA origami template and the silicon surface. In order to

evaluate the influence of the adsorption geometry on the determined strand break yield, an asymmetric pattern of protruding strands as shown in Figure 4b was used to quantify the relative yields of the two geometries by adsorption onto silicon surfaces and subsequent SAv binding. The AFM image in Figure 4a shows that SAv binding is observed for all DNA origami structures irrespective of their orientation, *i.e.*, face up or face down. The statistical analysis shown in Figure 4b reveals that about 83% of the DNA origami triangles adsorb face up and only ~17% face down. However, the shape of the histogram in Figure 3b, which does not show any deviations from a single Gaussian distribution in the form of shoulders or secondary peaks, indicates that the electrons are not shielded from the protruding strands by the template in the face-down geometry.

On the basis of these observations, we conclude that (i) even in the face-down configuration the Bt label is available for SAv binding, (ii) the orientation of the DNA origami template has no detectable effect on the dissociation yield, and (iii) the cleaved strands can be removed by the applied rinsing procedure (see Methods section) even though they are buried between the template and the surface.

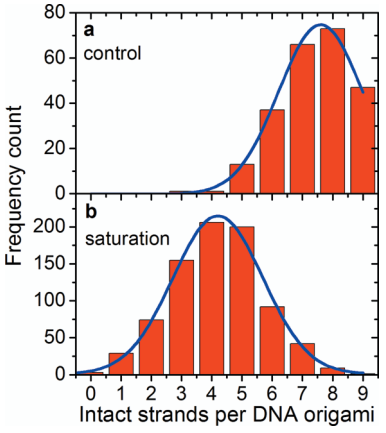

Figure 3. Histograms of the number of intact protruding strands per DNA origami (with initially nine SS-TT protruding strands, see Figure 2) (a) for a nonirradiated control sample and (b) after irradiation with $\Phi = 1.6 \times 10^{13}$ cm^{-2}. Both histograms correspond to a Gaussian distribution with a width of 2.8 and 3, respectively.

Disulfide Bond Dissociation *vs* DNA Strand Cleavage. In the present experimental system, the observed SSBs can result from the cleavage of the S−S bond, bond breakage within the $(CH_2)_6$ chain that connects the disulfide bridge with the DNA backbone, or damage to the DNA backbone itself (*i.e.*, P−O or C−O bond cleavage). To reveal details of the dissociation reactions, a new DNA origami structure (design D2) was introduced (Figure 5d). This design features three protruding strands with the sequence SS-TT-Bt and three protruding strands where the disulfide bridge has been omitted, *i.e.*, with the sequence TT-Bt. The asymmetric arrangement of the protruding strands on the DNA origami template enables the identification of the individual sequences. Electron irradiation again leads to a decrease in the number of specifically bound SAv molecules (Figure 5a−c). Statistical analysis, however, reveals a smaller number of SSBs for the TT sequence than for the SS-TT sequence, as can be seen in Figure 5d. The SS-TT DYs determined from the fit to the linear response regime for both designs D1 (with 9 disulfide-containing protruding strands) and D2 (with 3 disulfide-containing protruding strands) are shown in Figure 5e. Good agreement within the experimental errors is obtained. This indicates that the obtained DY does not depend on the number of potential cleavage sites per DNA origami structure within the accuracy of our measurement. The DY of the TT sequence, however, is drastically lower than the DY of the SS-TT target.

Since the DY of the disulfide bond has already been measured for design D1, the SS-TT sequence can serve as a reference in design D2, thus enabling the relative determination of the DY of the TT sequence without

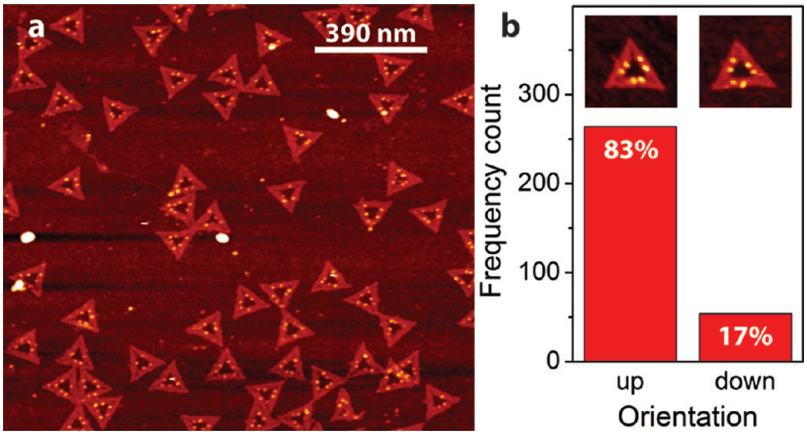

Figure 4. Determination of the adsorption geometry using DNA origami nanostructures with six protruding strands arranged in an asymmetric pattern. (a) The AFM image shows adsorbed DNA origami triangles after SAv binding. (b) Statistical analysis of DNA origami orientation. The insets give the face-up and face-down adsorption geometries.

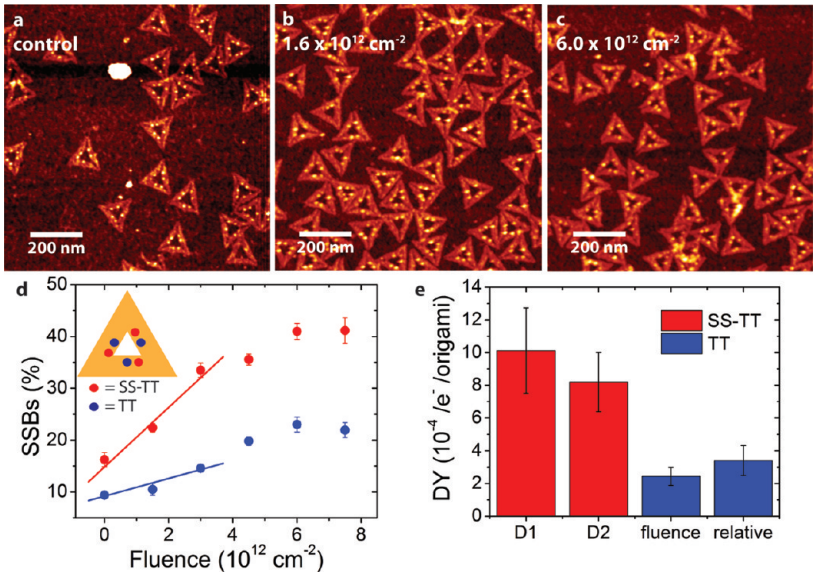

Figure 5. (a–c) AFM images of DNA origami samples with six protruding strands, three with the sequence SS-TT-Bt and three with the sequence TT-Bt: (a) control; (b, c) samples irradiated with 18 eV electrons at two different fluences in the linear (b) and the saturation regime (c). (d) Plot of the fluence dependence of the observed electron-induced strand breaks. (e) Comparison of the dissociation yields (DY) obtained for both designs D1 and D2 using the fluence method (SS-TT) and for design D2 using both the fluence and the relative method (TT). For the relative method, the data obtained at a fluence $\Phi = 3 \times 10^{12}$ cm^{-2} have been used.

TABLE 1. Gas-Phase Vertical and Adiabatic Ionization Potentials (IPs) and Electron Affinities (EAs) and Vertical Electron Detachment Energies (DEs) (in eV) of the Components of the Protruding Strands Shown in Figure 2 According to *ab Initio* Calculations at the MP2/6-311++G(d,p) Level of Theory

MP2/6-311++G**	Vert IP	Vert EA	Adia IP	Adia EA	Vert DE
Bt	8.54	−0.49	8.32	−0.53	−0.48
TT	9.05	−0.22	8.74	−0.48	−0.12
dTpdT	8.48	−0.06			
$CH_3O(CH_2)_6$-SS-$(CH_2)_6OCH_3$	8.58	−0.85	7.64	0.34	2.20
$CH_3O(CH_2)_6$-Bt	8.44	−0.52	8.26	−0.47	−0.44

the necessity of recording the full fluence dependence. For design D1, the DY has been calculated from the slope of the linear fit to the fluence (Φ) dependence of the relative number of strand breaks (SSB): $DY = \Delta SSB/\Delta\Phi$.

Within one recorded AFM image ($A = 4\ \mu m^2$) the electron fluence arriving at the individual DNA origami structures is assumed to be constant. Taking a control sample ($\Phi_0 = 0$) and an irradiated sample (Φ), we obtain for two different sequences protruding from the same DNA origami template $\Delta\Phi = \Phi - \Phi_0 = \Delta SSB_1/DY_1 = \Delta SSB_2/DY_2$.

With the previously determined yield of the reference sequence, DY_1, the DY of the second sequence can be expressed as $DY_2 = \Delta SSB_2/\Delta SSB_1 \times DY_1 = (SSB_{2,\Phi} - SSB_{2,0})/(SSB_{1,\Phi} - SSB_{1,0}) \times DY_1$.

In order to demonstrate the power of this approach, the DY for the TT sequence in design D2 has been determined both from the fluence dependence of the

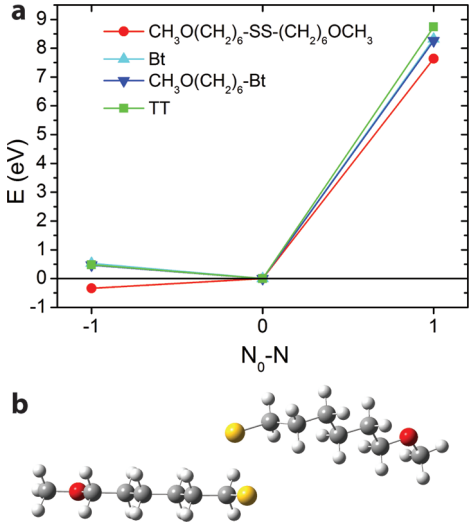

Figure 6. (a) Graphical representation of *ab initio* results showing the relative energies (in eV) of the cationic ($N_0 - N = 1$) and anionic ($N_0 - N = -1$) structures as a function of the excess of electrons relative to the neutral species ($N_0 - N$). The disulfide compound has the lowest adiabatic ionization potential and a positive adiabatic electron affinity. (b) Anionic disulfide linker stabilized by dissociation of the S–S bond.

SSBs (Figure 5d) and by applying the relative method at a fixed fluence of $\Phi = 3 \times 10^{12}$ cm^{-2}. The so-obtained DYs are in good agreement within the experimental errors, as is shown in Figure 5e. Therefore, using this relative method, the complete fluence dependence of the SSBs has to be recorded only once for a reference sequence. Then, the unknown DYs of all other target sequences protruding from the DNA origami template can be determined in a single irradiation experiment as

long as the applied fluence lies in the linear response regime.

The results presented above indicate that the SSBs preferentially occur by bond cleavage within the disulfide linker and only to a limited extend by damage to the DNA backbone within the TT sequence. Since all detected sequences contain the Bt modification, which is attached to the DNA via a $(CH_2)_6$ chain, it can further be concluded that also damage to the $(CH_2)_6$ chain within the disulfide linker can be neglected. This is supported by *ab initio* calculations using second-order Møller−Plesset perturbation theory (MP2) on all the relevant components of the protruding strands, *i.e.*, a stacked thymine dimer (TT), the disulfide linker (SS), and the Bt marker, both of the latter including the $(CH_2)_6$ chains. LEE-induced dissociation of the protruding strands can be initiated by either ionization or electron attachment. Consequently, the ionization potential (IP) and electron affinity (EA) of the specific components are important indicators for the underlying dissociation dynamics. Table 1 shows the vertical and adiabatic IPs and EAs along with the vertical detachment energies (DEs) of the relevant components of the detected sequences as calculated at the MP2/6-311++G(d,p) level of theory. Figure 6a shows the relative energies of the cationic and anionic structures compared to the neutral systems. The disulfide linker has the lowest adiabatic ionization potential and also the highest adiabatic electron affinity. Furthermore, it is energetically favorable for the anionic disulfide linker to undergo dissociation of the S−S bond, as shown in Figure 6b. The disulfide bond is thus the most probable cleavage site within the oligonucleotide, and its preferential cleavage can therefore be attributed to a direct interaction of the impinging electron with the two sulfur atoms.

CONCLUSIONS

The DNA origami template-based technique presented here makes it possible to visualize LEE-induced bond dissociations at a single-molecule level in complex, but well-defined target structures. We quantitatively determined and compared the number of LEE-induced bond dissociations for different target structures in a single experiment and at a single-molecule level. It thus offers a highly selective, comparatively fast, and efficient way to quantitatively evaluate the energy-dependent dissociation yields of individual chemical bonds.

Moreover, this novel approach holds great potential for applications in radiobiology since it enables the fast and reliable determination of DNA strand break yields with unprecedented control of the target primary and secondary structure, *i.e.*, nucleobase sequence and hybridization state. The dependence of the LEE-induced DNA cleavage on the nucleobase sequence has recently attracted considerable attention[20,31−35] and is believed to have strong implications for the design of novel radiosensitizing agents for cancer therapy.[36]

The presented scheme can further be extended to the investigation of DNA radiation damage in more complex systems such as biologically relevant DNA−protein complexes[37−39] by using templates with protein-modified protruding strands.[40] In addition, similar experiments can be performed with all kinds of radiation and in various environments, *e.g.*, photon irradiation in biological buffer. Thus, the presented DNA origami technique holds great potential for applications in radiation chemistry and biology.

METHODS

DNA Origami Synthesis. Triangular-shaped DNA origami structures were formed according to a modified version of Rothemund's method[22] with a molar ratio of 1:30 between the M13mp18 viral DNA (5 nM) and each of the staple strands in the 1 × TAE-Mg^{2+} (tris, 40 mM; EDTA, 2 mM; magnesium acetate, 12.5 mM; adjusted to pH 8.0 with acetic acid) in a total volume of 100 μL. The solution annealing was performed by gradually decreasing the temperature from 90 °C to 4 °C in 2 h on an Eppendorf Mastercycler Personal machine. After annealing, the sample was purified using an Amicon Ultra-0.5 mL filter (100 000 Da MWCO, 300*g* speed, 10 min) followed by washing with the 1 × TAE-Mg^{2+} (300 μL) to get rid of the excess staple strands. All DNA oligos were purchased from Metabion GmbH (Martinsried, Germany). All oligos were either HPLC purified or FCP purified (unmodified staple strands). M13mp18 viral DNA was purchased from New England Biolabs, Inc. Centrifugal Amicon Ultra-0.5 mL filters (catalogue number: UFC510096) were purchased from Millipore.

DNA Origami Adsorption. A 5 μL amount of the DNA origami samples was incubated in 45 μL of 100 mM $MgCl_2$ 10 × TAE buffer on commercially available epi-polished p-Si(100) surfaces (about 1 cm^2 area) for 3 h. The high concentration of Mg^{2+} ions is required for the adsorption of the negatively charged DNA origami nanostructures onto the negatively charged native surface oxide. After incubation, the Si surfaces were dried in a N_2 stream after rinsing the samples with 3 × 4 mL of a 1:1 mixture of ethanol and Milli-Q water in order to dehydrate the adsorbed DNA origami and to remove salt adsorbates.

Electron Irradiation. Electron irradiation was performed using a commercial electron flood gun mounted in a TOF.SIMS 5 (ION-TOF GmbH). The dried samples were introduced into the UHV chamber (base pressure ~10^{-10} mbar) and left for about two hours to degas. The samples were then irradiated under 45° incidence at a working pressure of ~10^{-8} mbar with the flood gun operated at 20 V. The diameter of the electron beam was about 5 mm, and the beam current ranged from 5 to 10 nA. The charging of the oxidized sample surface under these conditions was measured to be about 1.7 V, resulting in an effective electron energy of ~18 eV. The energy distribution of the electrons was measured to have a width of ~4.7 eV fwhm.

Streptavidin Binding. After irradiation, the samples were extracted from the UHV chamber and rinsed again as described above in order to remove the cleaved strands. Then the samples were incubated for 2 min in a 50 nM solution of streptavidin (Sigma Aldrich) in 10 mM $MgCl_2$ 1 × TAE buffer and subsequently rinsed with 2 × 0.5 mL of the 1:1 ethanol/water mixture.

AFM imaging was performed after drying the samples in a N_2 stream. The SAv-Bt binding efficiency was determined to be 80−90%.

AFM Imaging. The dried samples were imaged by tapping-mode AFM in air using a MultiMode scanning probe microscope equipped with a NanoScope IIIa, a NanoScope IV, and a NanoScope V controller from Veeco Instruments, respectively, as well as a Bruker MultiMode 8 operated in ScanAsyst-HR mode. For tapping-mode imaging, soft tapping cantilevers with a spring constant of nominally 5 N/m and a tip radius of <10 nm have been used (Tap150Al-G from BudgetSensors), whereas ScanAsyst-HR imaging was performed using SCANASYST-AIR-HR cantilevers (from Bruker, nom. spring constant 0.4 N/m, nom. tip radius 2 nm).

Statistical Analysis. For each fluence, 4 to 17 images have been taken at different positions within an area of about 3 mm^2 located in the center of up to four identically treated samples. The number of strand breaks per DNA origami nanostructure has been obtained for each AFM image and then averaged over the individual images. Therefore, the error bars given in Figures 2 and 5 include not only statistical fluctuations but also variations in the electron fluence that result from the Gaussian shape of the electron beam. In total, between 126 and 1398 individual DNA origami nanostructures have been analyzed per fluence value.

***Ab Initio* Calculations.** All *ab initio* calculations have been achieved with the Gaussian09 program suite.[41] The ground-state geometries of all the investigated systems (*i.e.*, pure biotin (Bt), stacked thymine dimer (TT), stacked dithymidine phosphate (dTpdT) as well as Bt and a disulfide linker (SS), both including the $(CH_2)_6$ chains) were first optimized in the gas phase at the density functional level of theory using the 6-31+G(d,p) polarized basis set. The functional B3LYP has been used for pure Bt, Bt, and SS with the carbon chains, while the optimizations of TT and dTpdT have been performed with the B97-D functional that includes an empirical van der Waals term accounting for dispersion effects. Frequency calculations for each derivative have been performed with the same level of theory, and it has been verified that all structures correspond to true minima of the potential energy surface. Energy differences, such as ionization potential, electron affinity, and electron detachment energy, were calculated using the second-order Møller−Plesset perturbation method with the 6-311++G(d,p) basis set. For the energy calculations of anionic and cationic species, we used the spin-restricted open-shell theory. Vertical IPs and EAs were obtained for all systems from the difference in total energy between the neutral species and the radical cation and anion, respectively, all evaluated at the optimized geometry of the neutral species. The adiabatic IPs and EAs were calculated for all systems, except dTpdT, in the same way but using the total energy obtained from the optimized geometry of the cationic and anionic form, respectively. Finally, the electron detachment energy was estimated from the difference in total energy between the neutral species and its radical anion, both evaluated using the optimized anion structure.

Conflict of Interest: The authors declare no competing financial interest.

Acknowledgment. This work was supported by grants from the Carlsberg Foundation, the Danish National Research Foundation and the Danish Research Agency. I.B. and A.K. acknowledge financial support from the Deutsche Forschungsgemeinschaft and the Alexander von Humboldt Foundation, respectively. A.R. acknowledges financial support from the European Union's Seventh Framework Programme (FP7/2007-2013) under grant agreement no. 264115-STREAM. E.C. thanks the F.R.S.-FNRS (Fonds National de la Recherche Scientifique de Belgique) and the Communauté Française de Belgique (ARC contract).

Supporting Information Available: Scheme of the triangular DNA origami structure along with all modified oligonucleotide sequences. This material is available free of charge via the Internet at http://pubs.acs.org.

REFERENCES AND NOTES

1. Arumainayagam, C. R.; Lee, H.-L.; Nelson, R. B.; Haines, D. R.; Gunawardane, R. P. Low-Energy Electron-Induced Reactions in Condensed Matter. *Surf. Sci. Rep.* **2010**, *65*, 1–44.
2. Lu, Q. B. Cosmic-Ray-Driven Electron-Induced Reactions of Halogenated Molecules Adsorbed on Ice Surfaces: Implications for Atmospheric Ozone Depletion and Global Climate Change. *Phys. Rep.* **2010**, *487*, 141–167.
3. Boudaiffa, B.; Cloutier, P.; Hunting, D.; Huels, M. A.; Sanche, L. Resonant Formation of DNA Strand Breaks by Low-Energy (3 to 20 eV) Electrons. *Science* **2000**, *287*, 1658–1660.
4. Engmann, S.; Stano, M.; Matejcik, S.; Ingolfsson, O. The Role of Dissociative Electron Attachment in Focused Electron Beam Induced Processing: A Case Study on Cobalt Tricarbonyl Nitrosyl. *Angew. Chem., Int. Ed.* **2011**, *50*, 9475–9477.
5. Golzhauser, A.; Eck, W.; Geyer, W.; Stadler, V.; Weimann, T.; Hinze, P.; Grunze, M. Chemical Nanolithography with Electron Beams. *Adv. Mater.* **2001**, *13*, 806-+.
6. Ballav, N.; Schilp, S.; Zharnikov, M. Electron-Beam Chemical Lithography with Aliphatic Self-Assembled Monolayers. *Angew. Chem., Int. Ed.* **2008**, *47*, 1421–1424.
7. Ballav, N.; Thomas, H.; Winkler, T.; Terfort, A.; Zharnikov, M. Making Protein Patterns by Writing in a Protein-Repelling Matrix. *Angew. Chem., Int. Ed.* **2009**, *48*, 5833–5836.
8. Turchanin, A.; Beyer, A.; Nottbohm, C. T.; Zhang, X.; Stosch, R.; Sologubenko, A.; Mayer, J.; Hinze, P.; Weimann, T.; Goelzhaeuser, A. One Nanometer Thin Carbon Nanosheets with Tunable Conductivity and Stiffness. *Adv. Mater.* **2009**, *21*, 1233-+.
9. Turchanin, A.; Weber, D.; Buenfeld, M.; Kisielowski, C.; Fistul, M. V.; Efetov, K. B.; Weimann, T.; Stosch, R.; Mayer, J.; Golzhauser, A. Conversion of Self-Assembled Monolayers into Nanocrystalline Graphene: Structure and Electric Transport. *ACS Nano* **2011**, *5*, 3896–3904.
10. Bald, I.; Langer, J.; Tegeder, P.; Ingolfsson, O. From Isolated Molecules Through Clusters and Condensates to the Building Blocks of Life. *Int. J. Mass Spectrom.* **2008**, *277*, 4–25.
11. Bald, I.; Dabkowska, I.; Illenberger, E.; Ingolfsson, O. Energy Selective Excision of CN^- Following Electron Attachment to Hexafluoroacetone Azine $((CF_3)(2)C{=}N\text{-}N{=}C(CF_3)(2)$. *Phys. Chem. Chem. Phys.* **2007**, *9*, 2983–2990.
12. Hla, S. W.; Bartels, L.; Meyer, G.; Rieder, K. H. Inducing All Steps of a Chemical Reaction with the Scanning Tunneling Microscope Tip: Towards Single Molecule Engineering. *Phys. Rev. Lett.* **2000**, *85*, 2777–2780.
13. Maksymovych, P.; Sorescu, D. C.; Jordan, K. D.; Yates, J. T. Collective Reactivity of Molecular Chains Self-Assembled on a Surface. *Science* **2008**, *322*, 1664–1667.
14. Morgenstern, K. Isomerization Reactions on Single Adsorbed Molecules. *Acc. Chem. Res.* **2009**, *42*, 213–223.
15. Pascual, J. I.; Lorente, N.; Song, Z.; Conrad, H.; Rust, H. P. Selectivity in Vibrationally Mediated Single-Molecule Chemistry. *Nature* **2003**, *423*, 525–528.
16. Henningsen, N.; Franke, K. J.; Torrente, I. F.; Sehulze, G.; Priewisch, B.; Ruck-Braun, K.; Dokic, J.; Klamroth, T.; Saalfrank, P.; Pascual, J. I. Inducing the Rotation of a Single Phenyl Ring with Tunneling Electrons. *J. Phys. Chem. C* **2007**, *111*, 14843–14848.
17. Pimblott, S. M.; LaVerne, J. A. Production of Low-Energy Electrons by Ionizing Radiation. *Radiat. Phys. Chem.* **2007**, *76*, 1244–1247.
18. Nguyen, J.; Ma, Y.; Luo, T.; Bristow, R. G.; Jaffray, D. A.; Lu, Q.-B. Direct Observation of Ultrafast-Electron-Transfer Reactions Unravels High Effectiveness of Reductive DNA Damage. *Proc. Natl. Acad. Sci. U. S. A.* **2011**, *108*, 11778–11783.
19. Martin, F.; Burrow, P. D.; Cai, Z. L.; Cloutier, P.; Hunting, D.; Sanche, L. DNA Strand Breaks Induced by 0−4 eV Electrons: The Role of Shape Resonances. *Phys. Rev. Lett.* **2004**, *93*, 4.
20. Li, Z. J.; Cloutier, P.; Sanche, L.; Wagner, J. R. Low-Energy Electron-Induced DNA Damage: Effect of Base Sequence in Oligonucleotide Trimers. *J. Am. Chem. Soc.* **2010**, *132*, 5422–5427.

21. Sanche, L. Low Energy Electron-Driven Damage in Biomolecules. *Eur. Phys. J. D* **2005**, *35*, 367–390.
22. Rothemund, P. W. K. Folding DNA to Create Nanoscale Shapes and Patterns. *Nature* **2006**, *440*, 297–302.
23. Tørring, T.; Voigt, N. V.; Nangreave, J.; Yan, H.; Gothelf, K. V. DNA Origami: A Quantum Leap for Self-Assembly of Complex Structures. *Chem. Soc. Rev.* **2011**, *40*, 5636–5646.
24. Voigt, N. V.; Torring, T.; Rotaru, A.; Jacobsen, M. F.; Ravnsbaek, J. B.; Subramani, R.; Mamdouh, W.; Kjems, J.; Mokhir, A.; Besenbacher, F.; *et al*. Single-Molecule Chemical Reactions on DNA Origami. *Nat. Nanotechnol.* **2010**, *5*, 200–203.
25. Helmig, S.; Rotaru, A.; Arian, D.; Kovbasyuk, L.; Arnbjerg, J.; Ogilby, P. R.; Kjems, J.; Mokhir, A.; Besenbacher, F.; Gothelf, K. V. Single Molecule Atomic Force Microscopy Studies of Photosensitized Singlet Oxygen Behavior on a DNA Origami Template. *ACS Nano* **2010**, *4*, 7475–7480.
26. Wang, Y. F.; Tian, S. X.; Yang, J. L. Resonant Dissociative Electron Attachments to Cysteine and Cystine. *Phys. Chem. Chem. Phys.* **2011**, *13*, 15597–15602.
27. Anusiewicz, I.; Berdys-Kochanska, J.; Simons, J. Electron Attachment Step in Electron Capture Dissociation (ECD) and Electron Transfer Dissociation (ETD). *J. Phys. Chem. A* **2005**, *109*, 5801–13.
28. Weik, M.; Ravelli, R. B. G.; Kryger, G.; McSweeney, S.; Raves, M. L.; Harel, M.; Gros, P.; Silman, I.; Kroon, J.; Sussman, J. L. Specific Chemical and Structural Damage to Proteins Produced by Synchrotron Radiation. *Proc. Natl. Acad. Sci. U. S. A.* **2000**, *97*, 623–628.
29. Abdoul-Carime, H.; Cecchini, S.; Sanche, L. Alteration of Protein Structure Induced by Low-Energy (< 18 eV) Electrons. I. The Peptide and Disulfide Bridges. *Radiat. Res.* **2002**, *158*, 23–31.
30. Huels, M. A.; Boudaiffa, B.; Cloutier, P.; Hunting, D.; Sanche, L. Single, Double, and Multiple Double Strand Breaks Induced in DNA by 3−100 eV Electrons. *J. Am. Chem. Soc.* **2003**, *125*, 4467–4477.
31. Ray, S. G.; Daube, S. S.; Naaman, R. On the Capturing of Low-Energy Electrons by DNA. *Proc. Natl. Acad. Sci. U. S. A.* **2005**, *102*, 15–19.
32. Vilar, M. R.; do Rego, A. M. B.; Ferraria, A. M.; Jugnet, Y.; Nogues, C.; Peled, D.; Naaman, R. Interaction of Self-Assembled Monolayers of DNA with Electrons: HREELS and XPS Studies. *J. Phys. Chem. B* **2008**, *112*, 6957–6964.
33. Markus, T. Z.; Daube, S. S.; Naaman, R. Cooperative Effect in the Electronic Properties of Human Telomere Sequence. *J. Phys. Chem. B* **2010**, *114*, 13897–13903.
34. Li, Z. J.; Cloutier, P.; Sanche, L.; Wagner, J. R. Low-Energy Electron-Induced Damage in a Trinucleotide Containing 5-Bromouracil. *J. Phys. Chem. B* **2011**, *115*, 13668–13673.
35. Cauet, E. Unique Hole-Trapping Property of the Human Telomere Sequence. *J. Biomol. Struct. Dyn.* **2011**, *29*, 557–561.
36. Wang, C. R.; Lu, Q. B. Molecular Mechanism of the DNA Sequence Selectivity of 5-Halo-2′-Deoxyuridines as Potential Radiosensitizers. *J. Am. Chem. Soc.* **2010**, *132*, 14710–14713.
37. Falk, M.; Lukasova, E.; Kozubek, S. Chromatin Structure Influences the Sensitivity of DNA to Gamma-radiation. *BBA - Mol. Cell Res.* **2008**, *1783*, 2398–2414.
38. Falk, M.; Lukasova, E.; Kozubek, S. Higher-Order Chromatin Structure in DSB Induction, Repair and Misrepair. *Mutat. Res.-Rev. Mutat.* **2010**, *704*, 88–100.
39. Surdutovich, E.; Gallagher, D. C.; Solov'yov, A. V. Calculation of Complex DNA Damage Induced by Ions. *Phys. Rev. E* **2011**, *84*.
40. Rinker, S.; Ke, Y.; Liu, Y.; Chhabra, R.; Yan, H. Self-Assembled DNA Nanostructures for Distance-Dependent Multivalent Ligand-Protein Binding. *Nat. Nanotechnol.* **2008**, *3*, 418–422.
41. Frisch, M. J.; Trucks, G. W.; Schlegel, H. B.; Scuseria, G. E.; Robb, M. A.; Cheeseman, J. R.; Scalmani, G.; Barone, V.; Mennucci, B.; Petersson, G. A.; *et al*. *Gaussian 09*, Revision A.1 ed.; Gaussian, Inc.: Wallingford, CT, 2009.